Research Article

대한치과재료학회지 53(3) : 121-132, 2026
Korean Journal of Dental Materials (*Korean J Dent Mater*)
ISSN:2384-4434 (Print); 2384-3268 (Online)
Available online at http://www.kadm.org
http://dx.doi.org/10.14815/kjdm.2026.53.3.121

470 nm 가시광선 조사 하에서 4종의 구강 관련 세균에 대한 은 코팅 Ni-Ti-O 나노튜브의 표면 특성 및 항균 활성

문경숙[1], 오승한[1,2], 최은주[3,4*]

[1]원광대학교 치과대학 치과생체재료학교실
[2]원광대학교 치과대학 생체재료매식연구소
[3]원광대학교 치과대학 구강악안면외과학교실
[4]원광대학교 치과대학 원광치의학연구소

Surface characterization and antibacterial activity of silver-coated Ni-Ti-O nanotubes against four oral-associated bacteria under 470 nm visible-light irradiation

Kyoung-Suk Moon[1], Seunghan Oh[1,2], Eun-Joo Choi[3,4*]

[1]Department of Dental Biomaterials, College of Dentistry, Wonkwang University, Iksan, Republic of Korea
[2]The Institute of Biomaterials and Implant, Wonkwang University College of Dentistry, Iksan, Republic of Korea
[3]Department of Oral and Maxillofacial Surgery, College of Dentistry, Wonkwang University, Iksan, Republic of Korea
[4]The Wonkwang Dental Research Institute, College of Dentistry, Wonkwang University, Iksan, Republic of Korea

니켈-티타늄(NiTi) 합금 표면에 제작된 은 코팅 Ni-Ti-O 나노튜브(AGT)는 가시광 광촉매 활성을 나타내지만, 그 표면 화학적 특성과 구강 세균에 대한 항균 효능은 아직 명확히 밝혀지지 않았다. 본 연구에서는 EDX가 결합된 FE-SEM과 XPS를 이용하여 AGT의 표면 특성을 분석하였으며, NiTi, Ni-Ti-O 나노튜브(NTO) 및 AGT 표면의 470 nm 가시광선 조사 유무에 따른 항균 활성을 *Streptococcus sanguinis*, *Streptococcus mutans*, *Staphylococcus aureus*, *Enterococcus faecalis*를 대상으로 집락형성능(CFU) 시험(n = 6)으로 평가하고, 이원배치 분산분석(two-way ANOVA)과 Tukey 사후검정으로 분석하였다. 은 증착 후에도 나노튜브 구조는 유지되었으며(Ag, 5.81 ± 0.11 wt%), XPS 분석 결과 금속 상태의 은을 포함하는 $NiTiO_3$ 형태의 산화물 표면임을 시사하였다. 표면 처리와 광조사 요인은 *E. faecalis*를 제외한 모든 균주의 생균수에 유의한 영향을 미쳤으며, *E. faecalis*의 경우 광조사 요인만 유의하였다. *S. sanguinis*에서만 표면 × 광조사 간 유의한 교호작용이 검출되었다 ($p < 0.001$). 470 nm 광조사 하의 AGT는 NiTi 대비 *S. sanguinis* (53.7%)와 *S. aureus* (63.0%)에서 가장 큰 세균 감소를 나타내었다. *S. mutans*에서는 광조사된 NTO (45.6%)가 광조사된 AGT(31.3%)보다 큰 감소율을 보였다. 본 연구의 한계 내에서, 470 nm 조사 하의 AGT는 시험 대상 구강 관련 세균에 대해 항균 활성을 나타냈지만, NTO에 대한 Ag의 추가적인 효과는 균주에 따라 차이가 있었다.

색인단어 : NiTi 합금, 은 코팅 Ni-Ti-O 나노튜브, 470 nm 가시광선, 항균 활성

Kyoung-Suk Moon (ORCID: 0000-0001-6534-3045)
Seunghan Oh (ORCID: 0000-0002-7250-721X)

*Correspondence: Eun-Joo Choi (ORCID: 0000-0002-6981-8439)
460 Iksan-daero, Iksan, Jeonbuk 54538, Republic of Korea
Affiliation: Department of Oral and Maxillofacial Surgery, College of Dentistry, Wonkwang University, Iksan, Republic of Korea
Tel: +82-63-859-2921, Fax: +82-63-857-6982
E-mail: cejoms@wku.ac.kr

Received: Aug. 16, 2026; Revised: Aug. 28, 2026; Accepted: Aug. 28, 2026

Introduction

Nickel–titanium (NiTi) alloys are widely used in orthodontic wires, endodontic instruments, and implantable devices because of their superelasticity, shape-memory behavior, and favorable biocompatibility (1, 2). However, the high Ni content of the alloy raises concerns regarding Ni ion release resulting from electrochemical corrosion, while bacterial colonization of the alloy surface remains a potential risk in the oral environment (3-5). Surface modification offers a practical approach for addressing both concerns simultaneously. Anodization of NiTi produces vertically aligned Ni–Ti–O nanotube (NTO) arrays that increase the specific surface area, suppress Ni release, and support the adhesion and proliferation of osteogenic cells (6-9).

In addition to passive protection, oxide nanotubes exhibit photofunctional activity. Although TiO_2 requires ultraviolet excitation because of its wide bandgap (3.2 eV), the mixed oxide formed on NiTi contains $NiTiO_3$ phases with a narrower bandgap, enabling visible-light-driven photocatalysis (10-12). We previously reported that decorating NTO with plasmonic metal nanoparticles further sensitized the surface to 470 nm blue light: Au coating narrowed the band gap and enhanced photocatalytic antibacterial activity against *Staphylococcus aureus* (*S. aureus*) *and Pseudomonas aeruginosa* (*P. aeruginosa*) (13), and Ag coating reduced the band gap of the nanotubes from 3.19 eV to 2.75 eV, conferring methylene-blue degradation activity and antibacterial effects under 470 nm irradiation without cytotoxicity toward human mesenchymal stem cells (hMSCs) (14). The 470 nm wavelength is of clinical interest because it corresponds to the output of dental light-curing units that are universally available at the chairside (13, 14).

However, two questions remain unanswered. First, the surface chemistry of the Ag-coated nanotubes—including the elemental composition of the coated layer and the chemical states of Ti, Ni, O, and Ag—has not been characterized, despite its fundamental importance to both the photocatalytic mechanism and Ag-mediated antibacterial action. Second, the antibacterial evidence obtained thus far concerns a skin-derived reference strain and a nosocomial Gram-negative rod, and the response of bacteria that initiate and dominate infections associated with intraoral NiTi devices is unknown. *Streptococcus sanguinis* (*S. sanguinis*) and *Streptococcus mutans* (*S. mutans*) are primary colonizers of intraoral surfaces and contribute to early biofilm formation, whereas *Enterococcus faecalis* (*E. faecalis*) is strongly associated with persistent endodontic and peri-implant infections (15-17). Furthermore, previous comparisons relied on one-factor analyses, which cannot distinguish the independent contributions of the surface treatment and the light irradiation or detect a synergistic interaction between them.

This study extends our previous report (14), which described the fabrication and 470 nm antibacterial activity of the coating, in three ways. First, its surface chemistry has not previously been reported and is characterized here. Second, the antibacterial panel is broadened from *S. aureus* and *P. aeruginosa* (13, 14) to oral-associated species. Third, the earlier comparisons were single-factor, whereas the factorial design used here separates the surface and irradiation effects and tests their interaction.

The strain panel was restricted to Gram-positive species. NiTi serves in orthodontic archwires and endodontic instruments rather than implants, so the target devices are exposed to supragingival plaque (*S. sanguinis, S. mutans*) or the root canal (*E. faecalis*), with *S. aureus* as a reference organism (13, 14). Gram-negative organisms, including *P. aeruginosa*, were covered earlier (13); their omission here is a limitation.

Therefore, the aims of this study were (i) to characterize the surface morphology, elemental composition, and

chemical states of AGT by FE-SEM/EDX and XPS and (ii) to evaluate the antibacterial activity of NiTi, NTO, and AGT surfaces against four bacterial strains (*S. sanguinis, S. mutans, S. aureus, and E. faecalis*) with or without 470 nm visible light irradiation, using a two-factor factorial design. The null hypotheses were that neither the surface treatment nor the 470 nm irradiation would affect bacterial viability and that no interaction would exist between the two factors.

Materials and Methods

1. Specimen preparation

NTO were fabricated on a NiTi alloy as described previously (13, 14). In brief, NiTi foil (5 × 5 cm^2, thickness 0.127 mm) was polished sequentially with #600, #1200, and #2000 silicon carbide papers and anodized in an ethylene glycol electrolyte containing 0.2 w/v% ammonium fluoride (NH_4F, Sigma-Aldrich, St. Louis, MO, USA) and 1.0 vol% deionized water at 25 V for 60 min. The anodized specimens were rinsed with heptane (Sigma-Aldrich) for 5 min, cleaned ultrasonically in deionized water, dried at 60 ℃ overnight, and heat-treated at 400 ℃ for 3 h (heating and cooling rate, 1 K/min) to crystallize the oxide (NTO group). Ag was deposited onto the nanotubes by ion plasma sputtering (E-1030; Hitachi Co., Tokyo, Japan) for a sputtering duration of 60 s, yielding the Ag-coated nanotube (AGT) group (14). Polished NiTi plates served as controls (NiTi group). The specimens were cut to 1 × 1.5 cm^2 before the biological assays.

2. Surface characterization

The surface and cross-sectional morphologies of the NTO and AGT groups were examined by FE-SEM (S-4800; Hitachi Co., Tokyo, Japan) at an accelerating voltage of 15.0 kV. To quantify the effect of the Ag deposition on the tubular architecture, the inner diameter and the wall thickness of the nanotubes were measured on the top-view images and the tube length on the cross-sectional images, and the diameter of the Ag particles was measured on the top-view images of the AGT group, using ImageJ (v1.53; National Institutes of Health, Bethesda, MD, USA; n = 30 per measurement). The elemental composition of the AGT surface was quantified by EDX attached to the microscope at 15.0 kV, and the values are reported as mean ± standard deviation of the repeated measurements. The surface chemical states of all three experimental groups (NiTi, NTO and AGT) were analyzed by XPS (K-Alpha; Thermo Fisher Scientific Co., Waltham, MA, USA; monochromated Al Kα source, hν = 1486.6 eV; spot size 400 μm, pass energy 50 eV, step 0.1 eV). Ni 2p, Ti 2p, O 1s and C 1s core-level spectra were acquired for all three groups, whereas Ag 3d spectra were acquired for the AGT group only, because Ag was present in that group alone. The binding energies quoted in the text were referenced to the adventitious C 1s peak of each specimen at 284.8 eV.

3. Antibacterial CFU assay

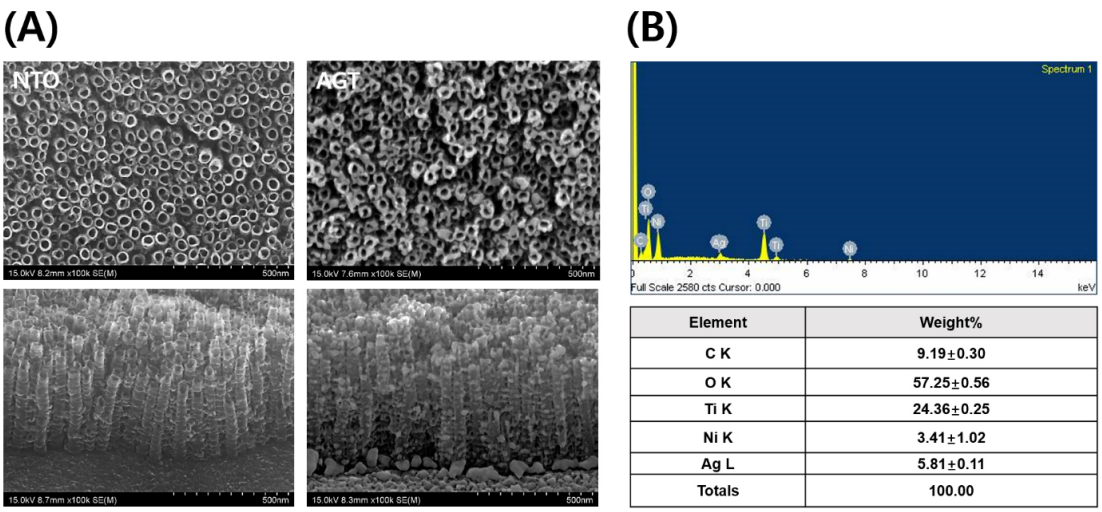
Four bacterial strains were used: *S. sanguinis* (ATCC 10556), *S. mutans* (ATCC 25175), *S. aureus* (ATCC 25923), and *E. faecalis* (ATCC 35038), all Gram-positive species (Table 1). *S. sanguinis*, *S. aureus*, and *E. faecalis* were cultured in tryptic soy medium (TSA; Difco, NJ, USA), and *S. mutans* was cultured in brain–heart infusion (BHI) medium, at 37 ℃ for 24 h, and each suspension was adjusted to 1 × 10^5 CFU/mL. A 50μL aliquot was inoculated onto each specimen and incubated at 37 ℃ for 6h. The specimens were then gently washed with phosphate-buffered saline (PBS), and the irradiated subgroups (NiTi/470, NTO/470, and AGT/470) were exposed to 470 nm visible light for 15 min using a light-emitting diode array (power density 5.5 mW/cm^2; specimen-to-LED distance, 4 cm) (13, 14), whereas the non-irradiated subgroups were kept in the dark. The center wavelength of 470 nm was selected because it coincides with the emission peak

of the dental LED light-curing units that are universally available at the chairside, and the LED array, the irradiance (5.5 mW/cm^2) and the specimen-to-source geometry followed those established in our previous studies of noble-metal-coated nanotubes so that the present data would be directly comparable with them (13, 14). The 15 min exposure corresponds to a radiant exposure of approximately 5 J/cm^2; this low-irradiance, longer-duration condition was chosen to sustain the photocatalytic reaction while keeping the irradiance more than two orders of magnitude below that delivered by a clinical curing unit (typically≥ 1,000mW/cm^2), so that a thermal contribution to the bacterial reduction was considered unlikely. Only this single dose was applied, and no dose–response relationship was established. Bacteria from each specimen were collected in 100μL of 1×PBS, serially diluted, plated on the corresponding agar(TSA for *S. sanguinis, S. aureus,* and *E. faecalis*; BHI agar for *S. mutans*), and incubated at 37 ˚C for 24 h, after which the colonies were counted. Six independent measurements per group (two independent experiments performed in triplicate) were obtained, and the percentage reduction in each experimental group was calculated against the mean of the batch-matched NiTi control.

Table 1. Bacterial strains and their characteristics

Characteristic	*Streptococcus sanguinis*	*Streptococcus mutans*	*Staphylococcus aureus*	*Enterococcus faecalis*
Abbreviation	SS	SM	SA	EF
ATCC No.	ATCC 10556	ATCC 25175	ATCC 25923	ATCC 35038
Media	TSA	BHI	TSA	TSA
Gram staining	Positive	Positive	Positive	Positive

TSA, tryptic soy agar; BHI, brain-heart infusion.



Element	Weight%
C K	9.19±0.30
O K	57.25±0.56
Ti K	24.36±0.25
Ni K	3.41±1.02
Ag L	5.81±0.11
Totals	100.00

Figure 1. (A) FE-SEM images (top and cross-sectional views) of the NTO and AGT groups. (B) EDX spectrum and quantitative elemental composition of the AGT surface, acquired at 15.0 kV. The labeled peaks correspond, from low to high energy, to C Kα (0.28 keV), Ti Lα (0.45 keV), O Kα (0.52 keV), Ni Lα (0.85 keV), Ag Lα (2.98 keV), Ti Kα (4.51 keV), Ti Kβ (4.93 keV) and Ni Kα (7.48 keV). Values in the table are mean ± standard deviation of the repeated measurements.

4. Statistical analysis

Data are expressed as mean ± standard deviation. For each outcome, a two-way analysis of variance (ANOVA) with the surface treatment (NiTi, NTO, AGT) and the 470 nm irradiation (dark, irradiated) as fixed factors was performed, followed by Tukey's post hoc tests for pairwise comparisons among the six groups. All analyses were performed using GraphPad Prism 8.4.3 (GraphPad Software, San Diego, CA, USA) at a significance level of $p < 0.05$.

Results

1. Surface morphology and elemental composition

FE-SEM observation (Figure 1(A)) showed that both the NTO and AGT groups retained a highly ordered, vertically aligned nanotubular architecture, and the tube openings remained patent after Ag deposition, with discrete Ag nanoparticles decorating the tube mouths and walls. The cross-sectional images confirmed that the nanotube layer was continuous and adhered well to the substrate in both groups. Quantitative image analysis showed that inner diameter decreased from 35.9 ± 3.0 nm (NTO) to 26.5 ± 3.0 nm (AGT), and wall thickness increased from 11.6 ±

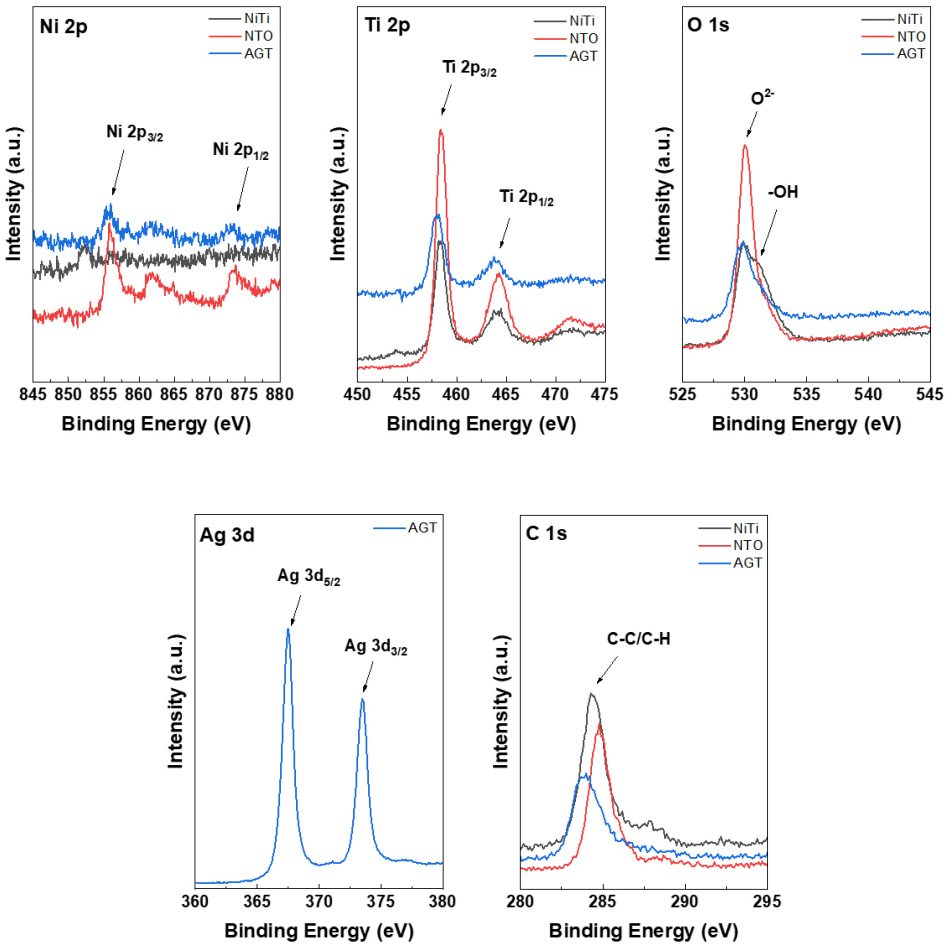


Figure 2. XPS core-level spectra of the experimental groups. Ni 2p, Ti 2p, O 1s and C 1s spectra are shown for NiTi, NTO and AGT; the Ag 3d spectrum is shown for AGT only, since Ag was present in that group alone. The spectra are plotted as acquired, whereas the binding energies quoted in the text were obtained after referencing the adventitious C 1s peak of each specimen to 284.8 eV.

1.6 nm to 21.2 ± 2.5 nm (n = 30 tubes per group, Mann–Whitney U test, $p < 0.001$ for both). The tube length was 717 ± 23 nm (NTO) and 728 ± 28 nm (AGT) (n = 30 tubes per group, Mann–Whitney U test, $p > 0.05$, not significant). The inner diameter decreased by 9.4 nm, whereas wall thickness increased by 9.6 nm after Ag deposition. The Ag particles on the AGT surface had a mean diameter of 24.0 ± 5.4 nm and were distributed mainly over the tube mouths and the upper part of the tube walls, so that the openings, although narrowed, remained open. These measurements were obtained from a single representative micrograph per group and therefore represent technical, not biological, replicates. EDX analysis of the AGT surface detected O (57.23 ± 0.56 wt%), Ti (24.36 ± 0.25 wt%), C (9.19 ± 0.30 wt%), Ag (5.81 ± 0.11 wt%), and Ni (3.41 ± 1.02 wt%), confirming that Ag was incorporated into the oxide surface at a reproducible level and that the outermost layer was strongly O- and Ti-enriched relative to the bulk alloy composition (Figure 1(B)).

2. Surface chemical states (XPS)

The XPS core-level spectra of the experimental groups are shown in Figure 2. Ni 2p, Ti 2p, O 1s and C 1s spectra were obtained for all three groups, and Ag 3d spectra for the AGT group. The Ti 2p and O 1s signals were markedly more intense on NTO and AGT than on the polished NiTi substrate, consistent with the formation of a thick anodic oxide layer, and on AGT these oxide-derived signals were attenuated relative to NTO, as expected when an overlying Ag deposit reduces the photoelectron yield from the underlying oxide. For the anodized surfaces, the Ti 2p spectrum contained a spin–orbit doublet at approximately 458.6 eV (Ti $2p_{3/2}$) and 464.3 eV (Ti $2p_{1/2}$), corresponding to Ti^{4+} in an oxide lattice. The Ni $2p_{3/2}$ peak appeared near 856 eV with a shake-up satellite, indicating that the Ni^{2+} species was consistent with a $NiTiO_3$-type oxide rather than with metallic Ni. The O 1s spectrum was dominated by lattice oxygen near 530.5 eV with a shoulder assigned to the surface hydroxyl groups. The Ag 3d spectrum contained a doublet at approximately 368.2 eV (Ag $3d_{5/2}$) and 374.2 eV (Ag $3d_{3/2}$) with a spin–orbit splitting of 6.0

Table 2. Two-way analysis of variance of surface treatment and 470 nm irradiation for each outcome

Outcome	Factor	F (df)	*p* value
S. sanguinis viable count	Surface	28.40 (2, 30)	< 0.001
	Irradiation	77.78 (1, 30)	< 0.001
	Surface × Irradiation	12.56 (2, 30)	< 0.001
S. mutans viable count	Surface	9.64 (2, 30)	< 0.001
	Irradiation	5.30 (1, 30)	0.028
	Surface × Irradiation	0.91 (2, 30)	0.413
S. aureus viable count	Surface	30.59 (2, 30)	< 0.001
	Irradiation	10.17 (1, 30)	0.003
	Surface × Irradiation	1.26 (2, 30)	0.297
E. faecalis viable count	Surface	0.75 (2, 30)	0.482
	Irradiation	18.64 (1, 30)	< 0.001
	Surface × Irradiation	0.24 (2, 30)	0.792

The surface factor had three levels (NiTi, NTO, AGT), and the irradiation factor had two levels (dark, 470 nm) for all outcomes; n = 6 per cell (two independent experiments in triplicate). Viable counts are CFU data for each bacterial strain. df, degrees of freedom.

eV, consistent with metallic Ag^0. The C 1s signal at 284.8 eV was attributed to adventitious carbon. Therefore, the XPS results indicate that the AGT surface consists of a Ni–Ti–O oxide bearing metallic Ag nanoparticles. Because the Ni 2p signal was weak and no diffraction analysis was performed, the XPS results are consistent with, but do not confirm, a crystalline $NiTiO_3$ phase.

3. Antibacterial activity

The two-way ANOVA results for the four strains are summarized in Table 2, and the group means with Tukey's groupings are presented in Table 3 and Figure 3. For *S. sanguinis*, the surface treatment ($F = 28.40$, $p < 0.001$), the irradiation ($F = 77.78$, $p < 0.001$), and their interaction ($F = 12.56$, $p < 0.001$) were all significant: the viable count

Table 3. Viable bacterial counts and percentage reduction after surface treatment and 470 nm irradiation

Outcome	Group	Viable count ($\times 10^4$CFU)	Reduction vs. NiTi (%)
S. sanguinis viable count	NiTi	632 (43)^{a}	—
	NiTi/470	573 (62)^{ab}	9.4 (8.4)
	NTO	525 (54)^{b}	16.9 (8.1)
	NTO/470	359 (36)^{c}	43.1 (6.2)
	AGT	596 (102)^{ab}	5.8 (15.9)
	AGT/470	293 (33)^{c}	53.7 (4.7)
S. mutans viable count	NiTi	1366 (257)^{a}	—
	NiTi/470	1213 (191)^{ab}	10.7 (8.2)
	NTO	1081 (165)^{abc}	18.9 (18.6)
	NTO/470	743 (182)^{c}	45.6 (8.9)
	AGT	942 (265)^{abc}	26.9 (30.9)
	AGT/470	867 (357)^{bc}	31.3 (37.5)
S. aureus viable count	NiTi	592 (72)^{a}	—
	NiTi/470	562 (83)^{a}	4.9 (12.7)
	NTO	483 (111)^{ab}	18.6 (14.4)
	NTO/470	340 (87)^{bc}	43.1 (10.8)
	AGT	344 (90)^{bc}	42.6 (9.9)
	AGT/470	225 (102)^{c}	63.0 (13.6)
E. faecalis viable count	NiTi	1137 (187)^{a}	—
	NiTi/470	841 (296)^{ab}	24.8 (28.0)
	NTO	1078 (131)^{ab}	4.8 (11.5)
	NTO/470	693 (212)^{b}	37.3 (24.1)
	AGT	1039 (214)^{ab}	8.9 (14.5)
	AGT/470	771 (244)^{ab}	30.8 (24.8)

Values are mean ± standard deviation (n = 6 per cell; two independent experiments in triplicate). Percentage reduction was calculated against the batch-matched NiTi control mean. Within each outcome, groups sharing no common superscript letter differ significantly (two-way ANOVA followed by Tukey' s post hoc test on viable counts, $p < 0.05$; GraphPad Prism 8.4.3).

on irradiated AGT (293 ± 33 × 10^4 CFU) was the lowest of all groups, corresponding to a 53.7% ± 4.7% reduction versus NiTi, and differed significantly from that of every group except irradiated NTO (43.1% ± 6.2% reduction), whereas non-irradiated AGT did not differ from the controls. For *S. mutans*, both main factors were significant (surface, $p < 0.001$; irradiation, $p = 0.028$) without interaction; irradiated NTO showed the largest reduction (45.6% ± 8.9%) and differed significantly from NiTi. For *S. aureus*, both main factors were significant (surface, $p < 0.001$; irradiation, $p = 0.003$) without interaction; AGT reduced the viable count significantly even in the dark (42.6% ± 9.9%), and irradiated AGT produced the greatest reduction among all groups (63.0% ± 13.6%). For *E. faecalis*, only the irradiation factor was significant ($F = 18.64$, $p < 0.001$); irradiated NTO was the only group that differed significantly from NiTi (37.3% ± 24.1% reduction), and the Ag coating conferred no additional benefit.

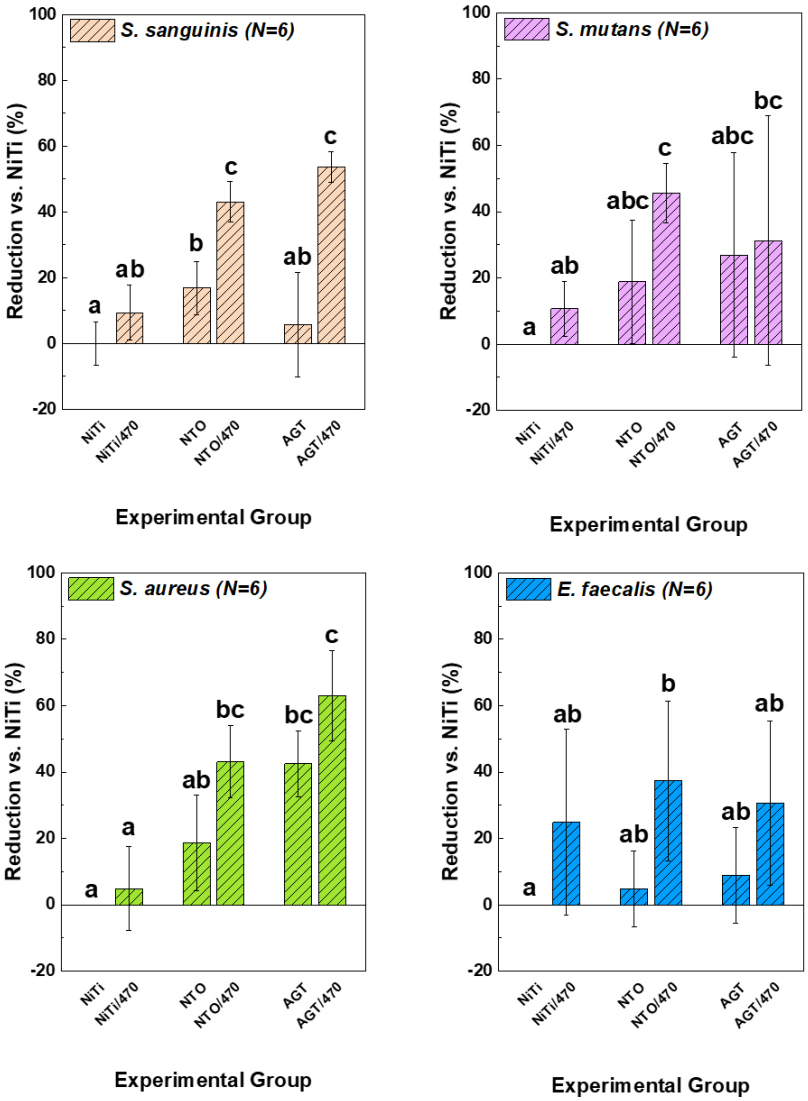


Figure 3. Percentage reduction in viable counts versus the NiTi control for *S. sanguinis*, *S. mutans*, *S. aureus*, and *E. faecalis* on the experimental groups with or without 470 nm irradiation (n = 6). Different letters indicate significant differences (two-way ANOVA with Tukey's post hoc test, $p < 0.05$).

Discussion

In this study we characterized the surface chemistry of AGT and evaluated their antibacterial performance against a panel of four bacterial strains using a factorial design. The null hypotheses were rejected for all strains except *E. faecalis*: the surface treatment and the 470 nm irradiation each independently reduced bacterial viability, and for *S. sanguinis*, a significant surface × irradiation interaction indicated that the Ag coating and the visible light interacted. The interaction was significant only for *S. sanguinis*, indicating that the contribution of Ag differed among bacterial species.

The EDX and XPS results provided a mechanistic foundation for these observations. An Ag loading of 5.81 wt% in the metallic Ag^0 chemical state supported two complementary antibacterial routes. The presence of metallic Ag may contribute to antibacterial activity through Ag^+ release, while Ag nanoparticles may also enhance visible-light photocatalysis of the underlying oxide (10–12, 18, 19). The reduction observed for non-irradiated AGT against *S. aureus* is compatible with a light-independent Ag effect, whereas the greater reduction after irradiation suggests an additional photocatalytic contribution. However, Ag^+ release and reactive oxygen species were not measured in this study, and these mechanisms remain to be verified experimentally. The XPS evidence for a $NiTiO_3$-type Ni^{2+}/Ti^{4+} oxide is consistent with the visible-light response of the uncoated nanotubes (10-12) and with the significant irradiation effects observed on the NTO surfaces.

The factorial analysis extends our previous one-factor comparisons in two ways (13, 14). This shows that the irradiation effect is a genuine main effect that persists across surface types, and it identifies for which organisms the Ag coating adds benefits beyond the photoactive oxide alone. The strain-dependence of the response is noteworthy. The two *streptococci* and *S. aureus* responded to both factors, whereas *E. faecalis* responded only to irradiation, with no measurable contribution from the Ag coating. *E. faecalis* is known for its exceptional tolerance to environmental stress and antimicrobial agents, which underlies its association with persistent endodontic infections (17). In the present data, this tolerance was expressed as the absence of any significant surface effect, although the underlying mechanism was not investigated here. The relatively large variability observed for *S. mutans* and *E. faecalis* may also have limited the ability to detect differences among groups.

The effect of Ag was strongly species-dependent. A significant surface × irradiation interaction was found only for *S. sanguinis*. In contrast, NTO/470 showed a larger mean reduction than AGT/470 for *S. mutans*, and no significant surface effect was observed for *E. faecalis*. *S. aureus* was the only strain for which AGT significantly reduced viability even without irradiation. Thus, Ag deposition did not consistently improve antibacterial activity over NTO.

The absolute magnitude of the effect also requires a cautious reading. The largest reductions obtained, 63.0% for *S. aureus* and 53.7% for *S. sanguinis*, correspond to only about 0.4 and 0.3 $\log_{10}$ respectively, whereas a reduction of at least 3 $\log_{10}$ (99.9%) is conventionally required before a surface or an agent is described as bactericidal. Effects of this size are unlikely to eliminate an established microbial burden on their own, and are more plausibly interpreted as a reduction in the initial adhesion and the early proliferation of colonizing bacteria. That is a meaningful but strictly adjunctive contribution, and the surface should be positioned as a complement to mechanical debridement and chemical antisepsis rather than as a replacement for either. Whether a reduction of this magnitude translates into a measurable clinical benefit, for example fewer white-spot lesions around orthodontic attachments or a lower rate of persistent intracanal infection, cannot be determined from an in vitro planktonic model and would require a clinical study.

The antibacterial evaluation was performed on planktonic cells of a single species allowed to adhere for 6 h, whereas the clinical problems that motivate this work, namely plaque accumulation on orthodontic appliances and persistent

intracanal infection, involve structured multi-species biofilms. A mature biofilm differs from the present model in ways that would be expected to reduce the efficacy observed here: the extracellular polymeric matrix restricts the diffusion of Ag^+ and quenches short-lived reactive oxygen species before they reach the cell envelope, the accumulated matrix and cell layers attenuate the light that reaches the photocatalytic surface, and cells in the deeper strata are metabolically less active and correspondingly less susceptible. Reactive species generated at an oxide surface also have a short diffusion range, so their action is largely confined to organisms in direct or near contact with the surface. The present data should therefore be read as evidence of activity against the initial colonization phase, and extrapolation to established biofilm is not warranted; evaluation in single- and multi-species biofilm models, with irradiation applied at defined biofilm ages, is the necessary next step.

From a clinical perspective, the effective wavelength of 470 nm coincides with the emission of ordinary dental light-curing units, which raises the possibility that the antibacterial function of the AGT surface could be reactivated chairside without dedicated equipment (13, 14). This remains a hypothesis rather than a demonstrated property. The present study applied a single irradiation episode and did not assess the retention of Ag after repeated irradiation, the stability of the coating in a simulated oral environment, or the durability of the antibacterial effect over successive cycles, so repeated-activation experiments with quantification of the residual Ag are required before reactivation at recall visits can be proposed as a clinical procedure. The reductions achieved here (up to 63% for *S. aureus* and 54% for *S. sanguinis* after a single 15 min exposure) were obtained against planktonic cells adherent for 6 h; because early colonizers such as *S. sanguinis* initiate the plaque community on intraoral surfaces (15, 16), suppressing their initial attachment phase is a rational target for controlling infection associated with intraoral NiTi devices. In a previous study, live/dead and MTT assays performed under a comparable 470 nm irradiation condition, with a 10 min exposure, showed no significant adverse effect on hMSC viability (14). The 15 min exposure used in the present work was not itself evaluated for cytocompatibility, and the effect of repeated blue-light activation on host cells has not been examined; both remain to be verified.

Several limitations should be considered. The antibacterial assay was limited to single-species planktonic cultures and a single irradiation condition, and therefore neither mature biofilm activity nor a dose–response relationship was evaluated. Ag^+ release and reactive oxygen species were not measured, so the proposed antibacterial mechanisms remain indirect. In addition, only Gram-positive bacteria were included, and the stability of the Ag coating and antibacterial response after repeated irradiation were not examined. Cytocompatibility under the 15 min irradiation condition also remains to be established. Finally, the observed reductions were relatively modest and should be interpreted as an adjunctive antibacterial effect rather than a bactericidal response.

Conclusion

Ag deposition preserved the Ni–Ti–O nanotubular structure and produced a surface containing metallic Ag. Both surface treatment and 470 nm irradiation affected bacterial viability, but the contribution of Ag varied among species. The largest mean reduction under irradiation was observed for *S. sanguinis*, whereas NTO alone performed similarly or better for *S. mutans* and *E. faecalis*. These findings indicate that Ag-coated NTO can provide light-responsive antibacterial activity, but its advantage over uncoated NTO is not universal. Further studies using biofilm models and repeated irradiation are needed to determine its potential for dental application.

Acknowledgements

This paper was supported by Wonkwang University in 2025.

References

1. Li YC, Wang FH, Shang JX. Ab initio study of oxygen adsorption on the NiTi (110) surface and the surface phase diagram. Corros Sci. 2016;106:137-46.
2. Gill P, Musaramthota V, Munroe N, Datye A, Dua R, Haider W, McGoron A, et al. Surface modification of Ni-Ti alloys for stent application after magneto electropolishing. Mater Sci Eng C. 2015;50:37-44.
3. Liu Y, Ren Z, Bai L, Zong M, Gao A, Hang R, et al. Relationship between Ni release and cytocompatibility of Ni-Ti-O nanotubes prepared on biomedical NiTi alloy. Corros Sci. 2017;123:209-16.
4. Gao A, Hang R, Bai L, Tang B, Chu PK. Electrochemical surface engineering of titanium based alloys for biomedical application. Electrochim Acta. 2018;271: 699-718.
5. Sun Y, Rong Y, Zhao Y, Yao X, Hang R. The influence of substrate electropolishing on anodization behavior, corrosion resistance, cytocompatibility and antibacterial ability of NiTi alloy. Mater Lett. 2020;268:127631.
6. Hang R, Liu Y, Liu S, Bai L, Gao A, Zhang X, et al. Size-dependent corrosion behavior and cytocompatibility of Ni-Ti-O nanotubes prepared by anodization of biomedical NiTi alloy. Corros Sci. 2016;103:173-80.
7. Hang R, Zhao F, Yao X, Tang B, Chu PK. Self-assembled anodization of NiTi alloys for biomedical applications. Appl Surf Sci. 2020;517:146118.
8. Lee PP, Cerchiari A, Desai TA. Nitinol-based nanotubular coatings for the modulation of human vascular cell function. Nano Lett. 2014;14:5021-8.
9. Hang R, Huang X, Tian L, He Z, Tang B. Preparation, characterization, corrosion behavior and bioactivity of Ni_2O_3 -doped TiO_2 nanotubes on NiTi alloy. Electrochim Acta. 2012;70:382-93.
10. Qu Y, Zhou W, Ren Z, Du S, Meng X, Tian G, et al. Facile preparation of porous $NiTiO_3$ nanorods with enhanced visible-light-driven photocatalytic performance. J Mater Chem. 2012;22(32):16471-6.
11. Shu X, He J, Chen D. Visible-light induced photocatalyst based on nickel titanate nanoparticles. Ind Eng Chem Res. 2008;47:4750-3.
12. Allahverdiyev AM, Abamor ES, Bagirova M, Rafailovich M. Antimicrobial effects of TiO_2 and Ag_2O nanoparticles against drug-resistant bacteria and leishmania parasites. Future Microbiol. 2011;6:933-40.
13. Moon KS, Bae JM, Oh S, Choi EJ. Enhanced photocatalytic antibacterial activity of Au-coated Ni-Ti-O nanotubes for biomedical applications. Mater Chem Phys. 2024;314:128910.
14. Moon KS, Jeong CS, Oh S, Choi EJ. Visible light mediated photocatalytic activity and antibacterial effect of Ag coated NiTiO nanotubes. Korean J Dent Mater. 2024;51(4):203-14.
15. Kolenbrander PE, Palmer RJ Jr, Periasamy S, Jakubovics NS. Oral multispecies biofilm development and the key role of cell-cell distance. Nat Rev Microbiol. 2010;8(7):471-80.
16. Loesche WJ. Role of *Streptococcus mutans* in human dental decay. Microbiol Rev. 1986;50(4):353-80.
17. Stuart CH, Schwartz SA, Beeson TJ, Owatz CB. *Enterococcus faecalis*: its role in root canal treatment failure and current concepts in retreatment. J Endod. 2006;32(2):93-8.
18. Chernousova S, Epple M. Silver as antibacterial agent: ion, nanoparticle, and metal. Angew Chem Int Ed Engl. 2013;52(6):1636-53.
19. Liao J, Mo A, Zhu Z, Quan Y. Antibacterial titanium plate deposited by silver nanoparticles exhibits cell compatibility. Int J Nanomedicine. 2010;5:337-42.

Research Article

Surface characterization and antibacterial activity of silver-coated Ni-Ti-O nanotubes against four oral-associated bacteria under 470 nm visible-light irradiation

Kyoung-Suk Moon[1], Seunghan Oh[1,2], Eun-Joo Choi[3,4]*

[1]*Department of Dental Biomaterials, College of Dentistry, Wonkwang University, Iksan, Republic of Korea*
[2]*The Institute of Biomaterials and Implant, Wonkwang University College of Dentistry, Iksan, Republic of Korea*
[3]*Department of Oral and Maxillofacial Surgery, College of Dentistry, Wonkwang University, Iksan, Republic of Korea*
[4]*The Wonkwang Dental Research Institute, College of Dentistry, Wonkwang University, Iksan, Republic of Korea*

Ag-coated Ni-Ti-O nanotubes (AGT) fabricated on nickel-titanium (NiTi) alloys exhibit visible-light photocatalytic activity; however, their surface chemistry and antibacterial efficacy against oral bacteria remain unclear. In this study, the surface characteristics of AGT were examined using FE-SEM with EDX and XPS, and the antibacterial activities of NiTi, Ni-Ti-O nanotube (NTO), and AGT surfaces with or without 470 nm visible-light irradiation were evaluated against *Streptococcus sanguinis*, *Streptococcus mutans*, *Staphylococcus aureus*, and *Enterococcus faecalis* by a colony-forming unit assay (n = 6) and analyzed by two-way ANOVA with Tukey's post hoc tests. The nanotubular architecture was preserved after Ag deposition, although the tube openings narrowed (Ag, 5.81 ± 0.11 wt%), and XPS indicated a $NiTiO_a$-type oxide surface bearing metallic Ag. The surface and irradiation factors significantly affected the viable counts of all strains, except *E. faecalis*, for which only irradiation was significant. A significant surface × irradiation interaction was detected only for *S. sanguinis* ($p < 0.001$). Irradiated AGT produced the largest reduction versus NiTi in *S. sanguinis* (53.7%) and *S. aureus* (63.0%). For *S. mutans*, however, irradiated NTO produced a larger mean reduction (45.6%) than irradiated AGT (31.3%). Within the limitations of this study, AGT under 470 nm irradiation showed antibacterial activity against the tested oral-associated bacteria, but the additional effect of Ag over NTO varied among strains.

Keywords : NiTi alloy, Ag-coated Ni-Ti-O nanotubes, 470 nm visible light, Antibacterial activity